DESIGN AND PRELIMINARY CHARACTERIZATION OF A 5 KW HALL THRUSTER PROTOTYPE

L. Biagioni [1], M. Saverdi [2], M. Berti [1], U. Cesari [2], and M. Andrenucci [1]

(1) Centrospazio-CPR, Pisa (Italy)
(2) Alta S.p.A., Via A. della Gherardesca 5, I-56121, Pisa (Italy)
Tel. +39 050 985072, e-mail: alta@alta-space.com

ABSTRACT

A nominally 5 kW Hall Effect Thruster (HET) prototype has been recently designed and built by Alta and Centrospazio-CPR, with the purpose of performing a wide range parametric exploration of the main engineering and physical aspects relevant to these propulsion technology. The thruster prototype was designed in such a way to be easily reconfigured and modified, in order to allow for different design and technology solutions to be implemented and tested on a quick and inexpensive system. The prototype was sized according to the well-known scaling relations which were developed in the former Soviet Union during the past decades, and which are presently being used for preliminary sizing also by Western teams: no attempt to optimise the design was performed. The result was a relatively prototypal thruster, which is however including (in the present configuration) a few non conventional features. During 2001 and 2002 the thruster underwent a number of experimental tests in order to characterize its main features, which include the magnetic design (B field shape and intensity in the discharge region, with a comparison to FEM predictions), the thermal design, the electrical discharge parameters, etc: these results will be herein presented. Firing characterization was performed in Alta's IV-4 test facility, a 2 m dia. 4 m length AISI 316 L vacuum chamber, equipped with a set of 7 tailored cryopumping surfaces: the selected set-up is characterized by a measured xenon pumping speed of about 70,000 l/s.

1. INTRODUCTION

The development of a new HET is a complicate and time consuming process, involving different design stages involving analytical, numerical and experimental activities, each one refining the thruster configuration and improving the accuracy of the predicted thruster performance.

Usually the first step in this process is scaling the thruster geometry according to some first order preliminary design method, optimising the target performance in order to achieve (at a given operating power) a target I_{sp}, maximum efficiency, and a satisfactory lifetime. This is a very important design phase, and proper preliminary identification of the thrusters parameters is extremely important for a successful thrusters development.

The successive design iterations are mainly employing computer simulation tools, which are useful in order to refine the magnetic field topology and the thruster layout, thus matching the design goals and optimising the operating parameters around their design values, while reducing plasma losses and especially thermal dissipation and erosion. These designs steps are verified during short duration experimental tests, intended at demonstrating specific design choices and ideas.

Finally, once the configuration is nearly frozen and the achievement of the design goals is experimentally proven, the design efforts concentrate on refining components and materials in order to reduce the mass of the thruster and increasing its reliability. Once these goals are satisfactorily achieved, the thruster can move on towards its final qualification.

It's understood that this design loop can be iterated as many times as required to converge to the desired performance, while specifications, data and hints are exchanged between the different design stages or they are derived from previous design experiences and experimental data. So far different scaling methods have been proposed by various design teams, mainly based on Russian design experience, extrapolation of existing experimental data and application of non-dimensional analysis of the equations governing thruster physics. Similarly a large variety of software codes have been developed and applied to HET design, often proving to have a fair agreement with experimental data.

Nonetheless, some significant issues are still open in this type of design approach. For instance scaling laws are not available for all the operating parameters, and have poor accuracy with respect to some key technological aspects (e.g. propellant injection conditions, cathode position, insulation requirements etc.) which, although usually considered to be of secondary relevance in the schematic models used for preliminary design, do play a fundamental role for actually stable, efficient and long life operation of HET.

In this respect, open literature is usually offering little help, mostly because these aspects are part of proprietary industrial know-how, or because they are assumed as an established "best practice" from Russian heritage and not further questioned. All the above aspects make the very first design iteration critical but important in order to gain basic information and to unveil technical issues that should be addressed before going through a more detailed and challenging design steps.
As a step towards a better understanding of these design issues, Alta and Centrospazio have recently designed and tested a simple multi-kW HET prototype (with a nominal operating power of 5 kW). The thrusters configuration features an extended acceleration zone with dielectric walls (SPT-type). The main goal of this activity was to lay the foundation for the development of a more mature (and better performing) high power HET prototype to be used for validation of Alta new large EP test facility in late 2003, supporting the preliminary design hypothesis and validating the numerical tools. Therefore no optimisation for the configuration and materials was attempted at this stage and was left to the following design iterations and evolution.
As a second objective, this development and test undertaking was also expected to support Alta commercial testing activities for external customers, evidencing critical aspects and components for high power thrusters tests and possibly uncovering the evolution of failure modes which are more easily identified in a non optimised thruster while they are usually latent in advanced models. This type of experience is believed to be very useful for extending the ability of early detection and identification of thruster malfunctioning.

2. THRUSTER DESCRIPTION

The operation of a HET is based on the acceleration of a quasi-neutral plasma by the interaction of an axial electric field and a radial magnetic field. The magnetic field intensity is such to magnetize electrons but not high enough to magnetize heavier ions, thus inducing axial (mostly thrust-generating ions) and azimuthal (or Hall, mostly electrons) current components. Ionisation is achieved by electron bombardment in the in the high Hall current region.
Because of the highly interconnected and complex phenomena occurring in a Hall discharge, optimisation of a HET in order to maximise the performance is a difficult and time consuming task. In the case of Alta/Centrospazio 5 kW HET prototype no performance optimisation was attempted (even though the thrusters eventually achieved a fair performance level), but rather the thruster was designed in such a way to allow for quick and inexpensive reconfiguration and modifications, to study different design solutions and to provide a robust workhorse for training of personnel and students and for testing of new diagnostic and measurement techniques.

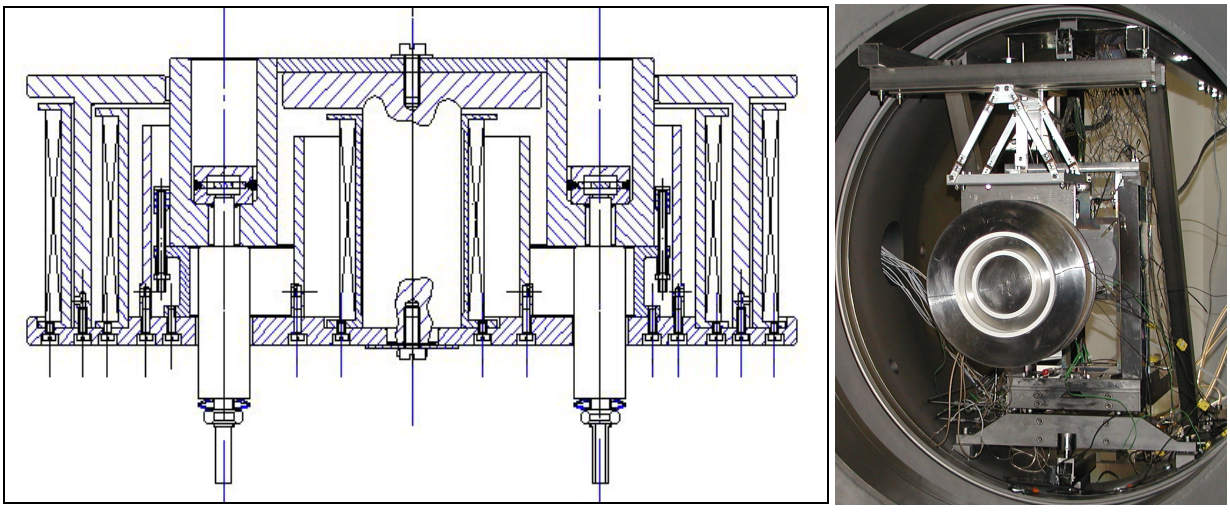

Fig. 1 The 5 kW HET prototype.

The thruster layout is very similar to University of Michigan P5 prototype ([1,2] which was taken as a reference), although with three independently powered axi-symmetrical coils (which allow to modify the shape of the magnetic field and investigate the behaviour of the plume) rather than the discrete pole configuration. The thruster discharge chamber has an external diameter of 172 mm: this value was obtained by interpolation of data from previous SPT-type HET. Although nominally designed for 5 kW, the preliminary sizing tool developed by Alta (based on an extended database of experimental points) indicates

for this thrusters a maximum efficiency operating point at a 7 kW power level, and a maximum thrust-to-power ratio operating point at 3 kW.
For the sake of simplicity, the anode piece configuration features an axial propellant injection (with an intermediate sect) and two parallel feeding lines: during the following firing tests this choice proved to be poorly performing, and a new anode is presently being manufactured. Commercial-grade carbon steel was used for the magnetic circuit, high temperature stainless steel for the anode piece, and high purity boron nitride for the discharge chamber. Finally a hollow cathode/neutralizer assembly manufactured by Qinetiq was fitted for the firing tests.

3. THE MAGNETIC CIRCUIT

The selection of a properly configured magnetic field is one of the fundamental aspects in the design of an effective HET [8,9]. In the case of a relatively high power thrusters, the main issues are not related to the possibility to achieve a sufficiently high intensity: as a matter of fact, for increasing thruster size, the peak magnetic field intensity is slightly decreasing or constant kept constant and the larger size reduces the risk of magnetic saturation of the pole material. On the other hand, the larger size introduces uncertainties on the uniformity of the achieved field and (as will be detailed below) the higher power increase the risk of thermally induced saturation during long duration firing tests.
The main requirements considered in the design of the magnetic circuit for the present prototype were as follows:

- Maximum magnetic field intensity on the thrusters exit plane ($B_{r\,max}$=150÷300 G)
- Uniform axial gradient $dB_r/dZ>0$ inside the discharge chamber to prevent instability phenomena of the plasma column
- Constrained position of the radial magnetic field half-maximum point
- Negligible axial magnetic field component

The first step in the magnetic circuit sizing process has been the evaluation of the ideal (no losses) equivalent reluctance of its components, in order to identify the nominal magneto-motive force required for operation. The magnetic circuit scheme is shown in Fig. 2, together with the equivalent electric circuit used to size the magnetic circuit coils.

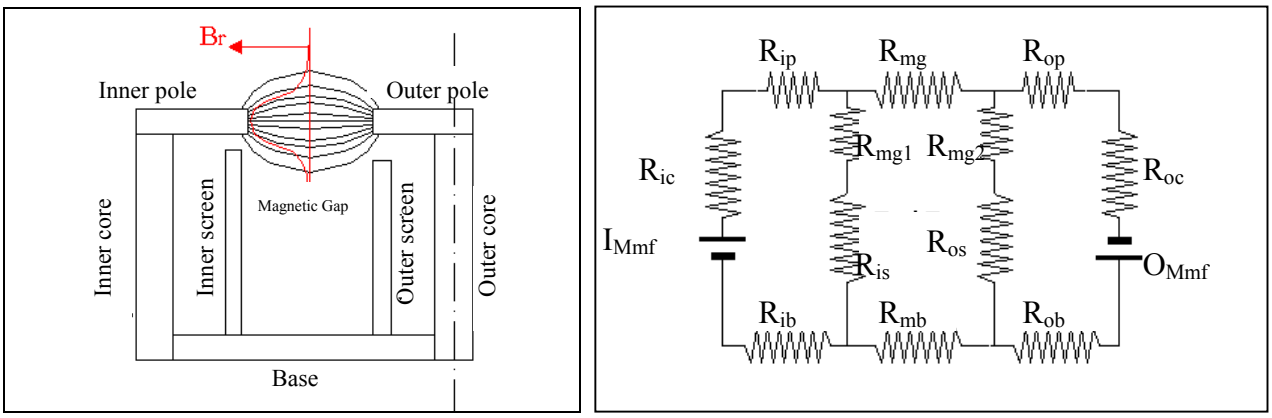

Fig. 2 Magnetic circuit and equivalent electric circuit.

The second step in the sizing process has been the FEM simulation of the of the magnetic circuit layout, in order to refine the results of the first approximation calculations and to better refine the field topology by adjusting the poles and internal screens configuration. The magnetic field simulation for the final thruster layout is shown in the Fig. 3. The peak magnetic field value from the FEM simulation is clearly lower than what predicted by the first order calculation, mostly because of the magnetic dispersion in front and on the sides of the thruster. The final topology is complying with the requirements: in particular nearly no radial field is present close to the anode, with a rapidly increasing distribution peaking on the exit plane; furthermore the axial component is much smaller than the radial one along the whole channel.

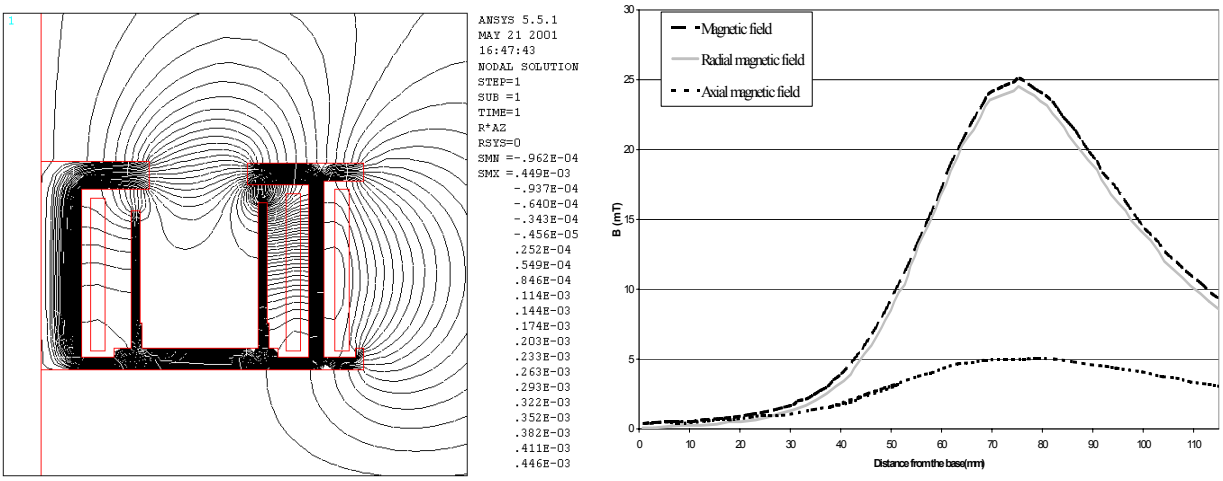

Fig. 3 Magnetic induction lines distribution (left) and value of the magnetic induction components along the channel centreline.

4. THERMAL DESIGN AND MODELLING

Both scaling formulae and experimental evidence indicate that HET efficiency (in the order of 50%÷60%) increases for increasing thruster power. Therefore the fraction of the discharge energy which is released on the thruster walls decreases (although the local surface load density may increase). Nevertheless, a correct thermal design is of paramount importance for HET thrusters operating for long duration in a steady mode, in order to:

- decrease the thermal load on the ceramic discharge chamber (which is particularly critical with respect to thermal gradient induced stresses and cracking);
- decrease the thermal load on the magnetic circuit elements, to avoid saturation of the poles (which induces plasma defocusing and performance loss) and overheating of the magnetic coils (which leads to increase in ohmic resistance and therefore dissipated power, and to possible damage of the wire electrical insulation layer);
- decrease the thermal load towards the spacecraft body, thus reducing integration and operation concerns and limitations.

The thermal design, usually performed through numerical models, also relies on a clever choice of materials with the proper mix of thermal conductivity and emissivity, and on a suitable geometrical arrangement of the thruster components/connections, in order to drive the heat flow away from the critical parts and to radiate it safely towards outer space.

Experimental tests performed on SPT-100 and SPT-140, allow (as a first approximation) to define the following thruster power balance [3,4,6]:

- 60% of the nominal power is released as plume kinetic energy;
- 20% is released as thermal dissipation on the discharge chamber walls;
- 10% is released inside the operating hollow cathode;
- 5% is needed for propellant ionisation;
- 5% is released as thermal dissipation on the anode surface.

In the present case of a nominally 5 kW thruster, and for the purpose of initial thermal modelling, the above power balance translates into a 1000 W surface heat load distributed on the discharge chamber walls and a 250 W load released on the anode. In addition, about 200÷300 W were expected to be dissipated by the magnetic coils, and were included to account for the separately driven magnets.

The thermal simulation was performed considering all thruster surfaces to radiate towards a uniform background at room temperature (accounting for the vacuum chamber walls). The thruster base (which would be connected to the thrust stand structure during the ground tests) was assumed not to be conducting heat away, and to have the same radiation boundary condition as the remaining surfaces: the mounting fixtures of the thruster were then designed in order to satisfy this assumption. As a result of these choices, the total dissipated power is assumed to be radiated away. Fig. 4 shows the computed thermal distribution: as expected the maximum temperature is reached on the discharge chamber inner wall lip, while the minimum temperature is maintained on the outer pole where the emitting surface is larger.

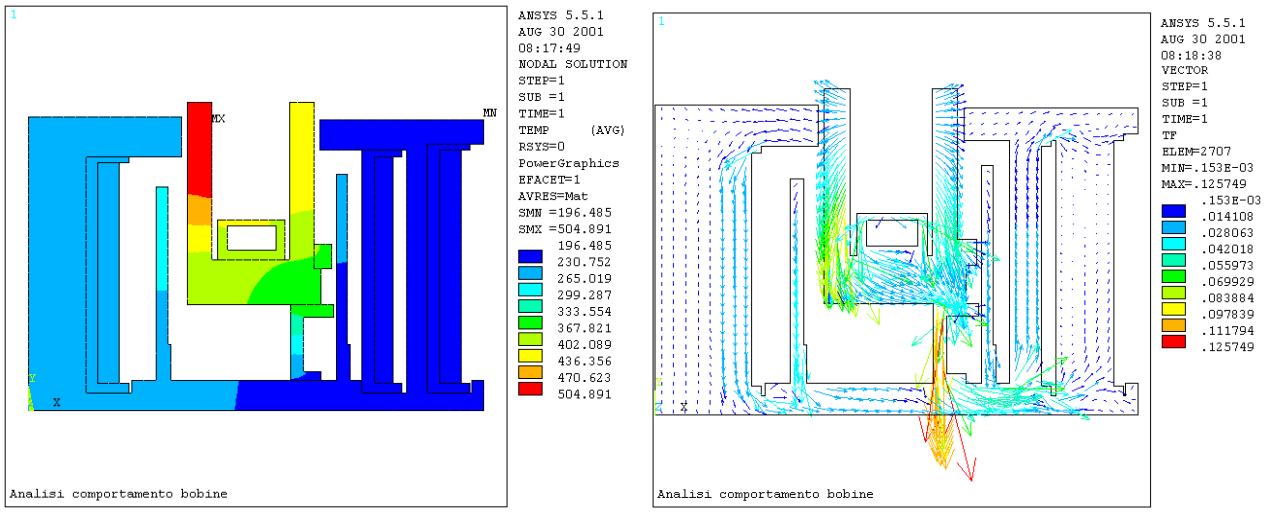

Fig. 4 Temperature and thermal flux distributions.

5. TEST FACILITY DESCRIPTION

Two different types of test were so far performed on the thruster prototype: ambient condition mapping of the magnetic field distribution (in order to validate the design and the results from numerical simulations) and thermal behaviour assessment and limited performance measurement during in-vacuum firing tests.

The magnetic field has been mapped using a simple three-axis device equipped with miniature Hall probes, featuring a ±400 G range. The results are shown in the following paragraphs.

The thruster firing tests were performed in Alta IV-4 facility, a 2 m dia. 4 m long diamagnetic stainless steel (AISI 316 L) chamber, equipped with 7 tailored, cold-head driven xenon pumping surfaces. Although the facility maximum pumping speed is about 130,000 l/s on Xe, during these tests the pumping system was arranged in the configuration for long duration tests, with smaller plates for higher endurance with respect to saturation of the cryo-surfaces: this limited the pumping speed to about 70,000 l/s on Xe. The dynamic pressure during thrusters operation (measured by two Xe calibrated Leybold-Inficon and one Alcatel ionisation gauges) was always between 2e-5 and 4e-5 mbar in Xe: this pressure level is probably not sufficiently low to state that the thrusters performance is un-affected by background gas entrainment, but acceptable for the purposes of this initial test campaign.

The chamber walls in front of the thruster exit plane were fully lined with high-purity, vacuum treated graphite plates in order to reduce (as far as possible) contamination and back-sputtering to the thruster: although not a concern for this specific test campaign, the high power firing tests were extremely useful for better characterizing graphite plate behaviour when exposed to a high plasma load. Pumping speed and back-sputtering rate were also positively affected by the shape of the water-cooled bi-conical target neutralizing the thruster plume.

The thruster was installed on a four-arm, one-axis thrust stand in a direct pendulum configuration (shown in Fig. 5). The thrust stand was adapted from a legacy arcjet experiment, and was not optimised for the different thrust-to-mass ratio of a high power HET: for this reason the achieved accuracy in thrust measurement is about 5%. The thruster was equipped with eleven type-K thermocouple in different positions inside and outside the thrusters assembly, and with current sensors to measure the discharge parameters. During firing tests the standard digitising frequency was 1 Hz, however ignition transients were digitised at 100 kHz in order to capture the in-rush currents. Discharge voltage was measured directly from the PSU output with low sample rate. Data, except voltages, were monitored in real time and recorded by the dedicated data acquisition and control system.

The thruster power system consisted of a 5 kW (500 V max, 14 A max) Huttinger PFG 5000 power supply directly connected to the anode: no filter unit was used during the tests herein presented. Five other small laboratory power supply units were used to separately drive the three coils, the cathode heater and the cathode keeper. The propellant feed system (supplying grade 4.8 xenon to the anode and cathode connections) consisted of commercial pressure regulators and of two Bronkhorst FCA mass flow controllers for the anode and the cathode lines. Mass flow rate accuracy was about 1%, mass flow controllers were factory calibrated on xenon at the beginning of the test activities.

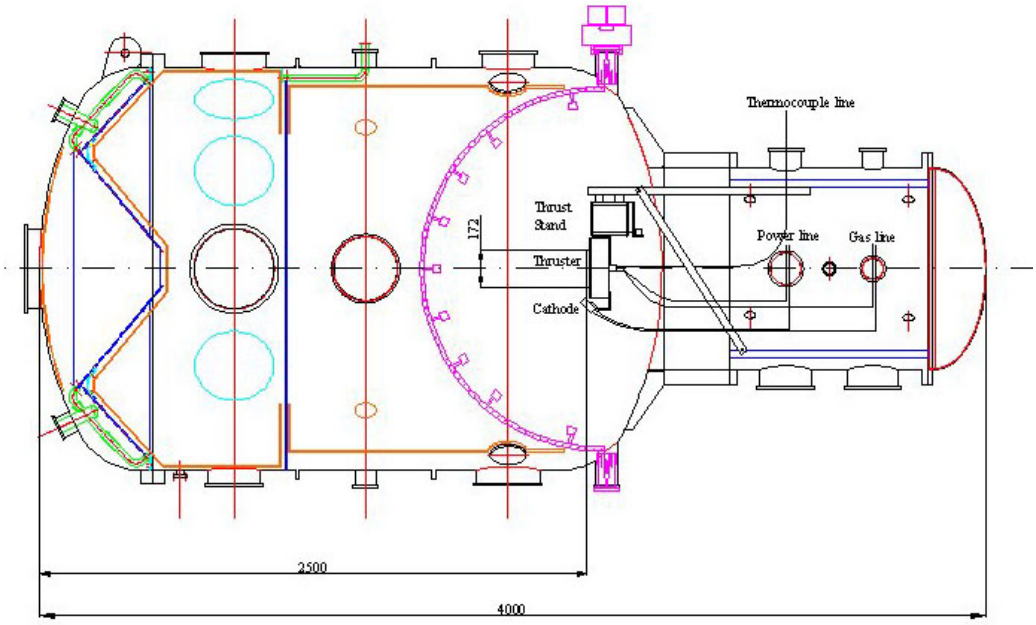

Fig. 5 Alta IV-4 test facility schematic.

6. RESULTS AND DISCUSSIONS

The magnetic field mapping showed good correspondence between the simulation and the actually realised field topology: magnetic induction is essentially radial between the polar expansions, where it reaches its maximum value, and almost zero near to the anode. A comparison of the computed and measured radial component is shown in Fig. 6, while the axial component is shown in Fig. 7.

The comparison between simulation and experimental results shows some difference in the maximum value of the magnetic induction, which in the real case is about 12 % lower than what predicted. Furthermore, the magnetic field near the anode is larger than predicted (Fig. 8 left). It is believed that this difference is induced by imperfect contact between the magnetic cores and expansions. By accounting for this fact (introducing a 0.2 mm gap between the magnetic components) the simulation results are better capturing the experiments in the peak region, although the shape of the field in the anode region is not properly modelled (Fig. 8).

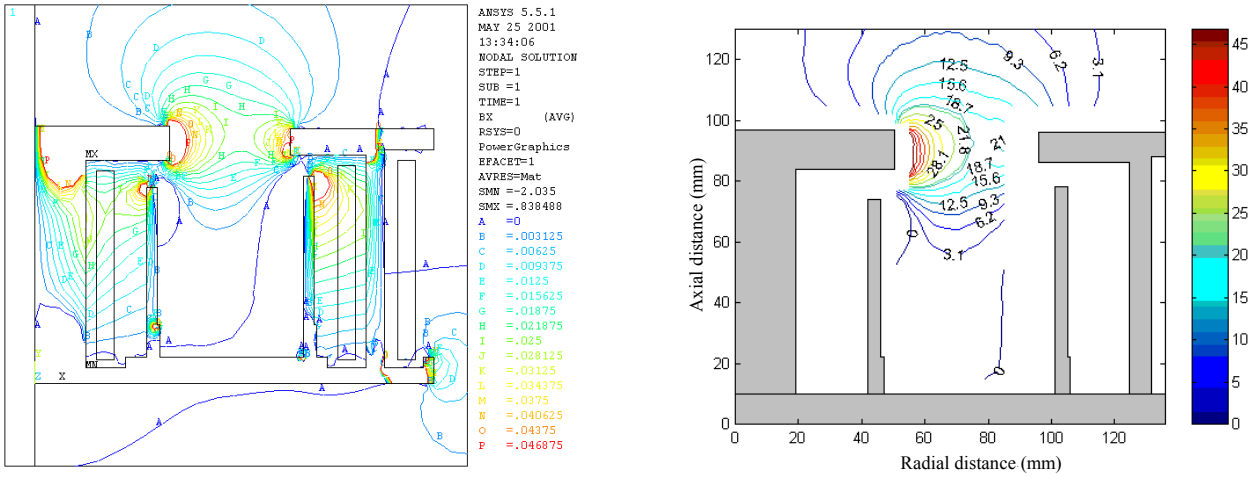

Fig. 6 Radial magnetic field component: numerical simulation (left) and experimental results (right).

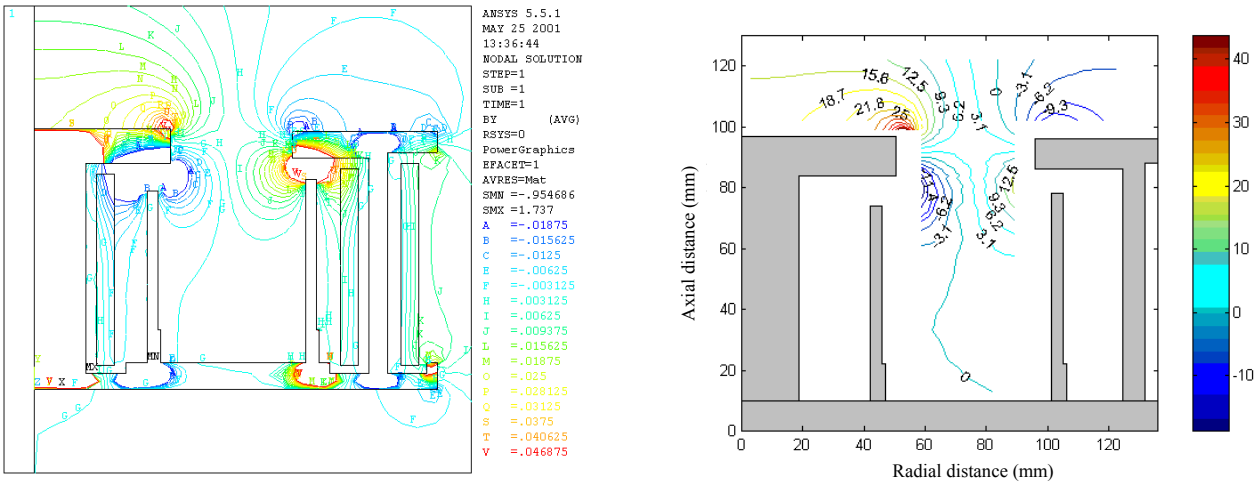

Fig. 7 Axial magnetic field component: numerical simulation (left) and experimental results (right).

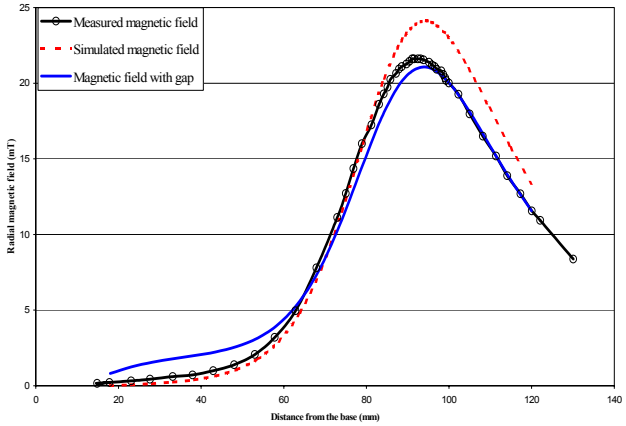

Fig. 8 Comparison between the simulated and measured radial magnetic field.

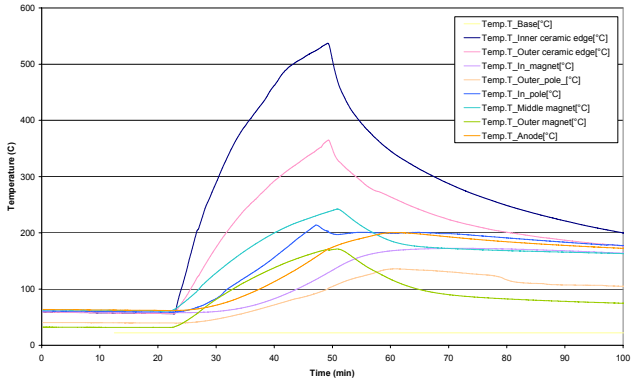

Fig. 9 Experimental temperature history in different positions, discharge power 3800 W, total power (discharge+magnets) 4250 W.

Temperature history during a 25 minutes run at 3.8 kW is shown in Fig. 9. The measured values, although qualitatively resembling the computed ones, are higher than expected (530 C and raising on the inner ceramic wall). In particular the most part of the ceramic wall heat load is apparently released on the inner wall: although this was expected (a 60-40 distribution was used in the FEM model respectively for the inner and outer walls), the experimental results show an even stronger unbalance.

The first approximation thermal assumptions used for the initial modelling (scaled from SPT-100 results) are not properly capturing the different operating conditions of the prototype. However the new results will be used in order to improve the FEM prediction capability, by properly identifying the boundary and coupling conditions of the various thruster components. It must also be noted that the thermal steady state was not

achieved during the 30 minutes runs which were the maximum allowed (at 4+ kW) by the facility in the chosen configuration. Longer runs will be performed over the next few months after improving the facility heat management lay out.

Performance results obtained during the preliminary test campaign are shown in Fig. 10 and Fig. 11. In particular, the graphs show performance parameters obtained with three different xenon anode mass flow rates: 6 mg/s, 8 mg/s and 10 mg/s. Cathode mass flow rate was fixed to 0.4 mg/s, no attempt to optimise the anode/cathode coupling was performed. Both anode and cathode mass flow rates were used to calculate the plotted specific impulse and efficiency; however only the main discharge power was considered to compute the thruster efficiency, not including magnetic coil dissipation (about 350 to 450 W).

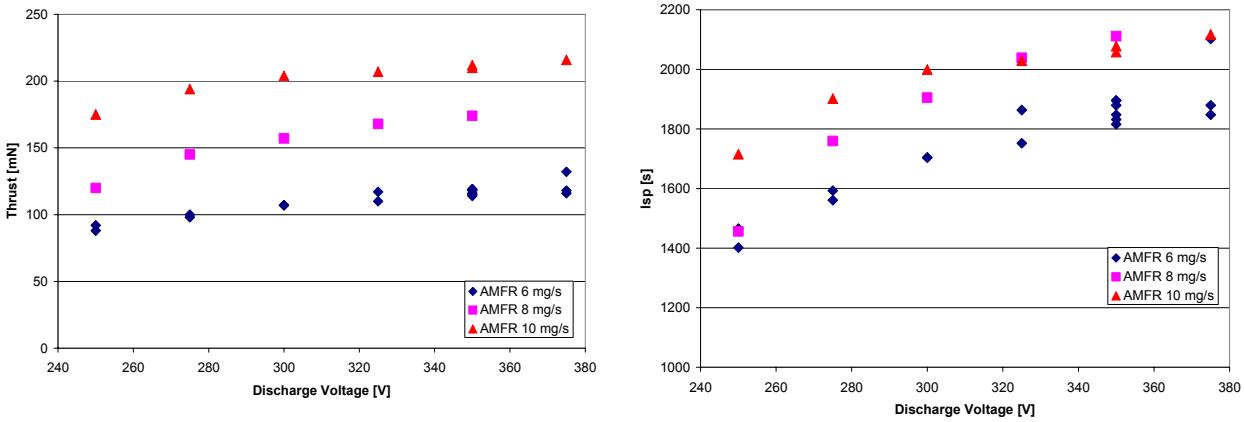

Fig. 10 Thrust (left) and specific impulse (right) vs discharge voltage.

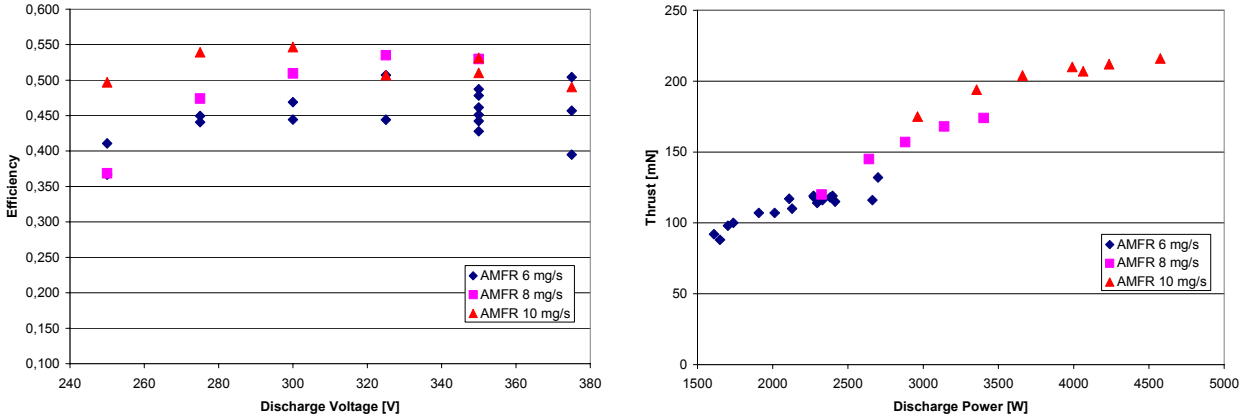

Fig. 11 Efficiency vs discharge voltage (left), thrust vs discharge power (right)

Although the test campaign mostly confirmed the expected behaviour (especially concerning the magnetic field topology and, to a lesser extent, the temperature distribution), the thruster operating conditions were relatively different from what initially expected. During thruster operation it can be seen that the bright region corresponding to propellant ionisation is quite deep into the channel (close to the anode) rather than being just below the thruster exit plane, as desired. This phenomenon induces an increase in ion losses at the walls (and a corresponding higher erosion, extending deep into the channel) with a consequent increase in axial electron current, and also an increase in the probability of double ionisation (since the already ionised propellant has a longer path through high electron current regions). Correspondingly, the measured discharge current is higher than expected for a given mass flow rate, and the anode efficiency is reduced.

This behaviour is believed to be caused by the propellant injection mode, which in this case is achieved through a series of simple axial orifices. DSMC simulations of both axial and radial neutral injection (with the same mass flow rate) in the acceleration chamber show that, in the axial injection case, the xenon jets are quickly expanding resulting in a lower number density and in an higher radial density gradient on the exit plane. On the other hand, in the radial injection case the neutral distribution is by far more homogeneous. For example, the same propellant density found on the exit plane in the case of radial injection, is achieved just 15 mm downstream of the anode when using simple axial orifices. In order to better understand this effect, a

new anode with radial injection is presently being manufactured and will be tested during the next few months.

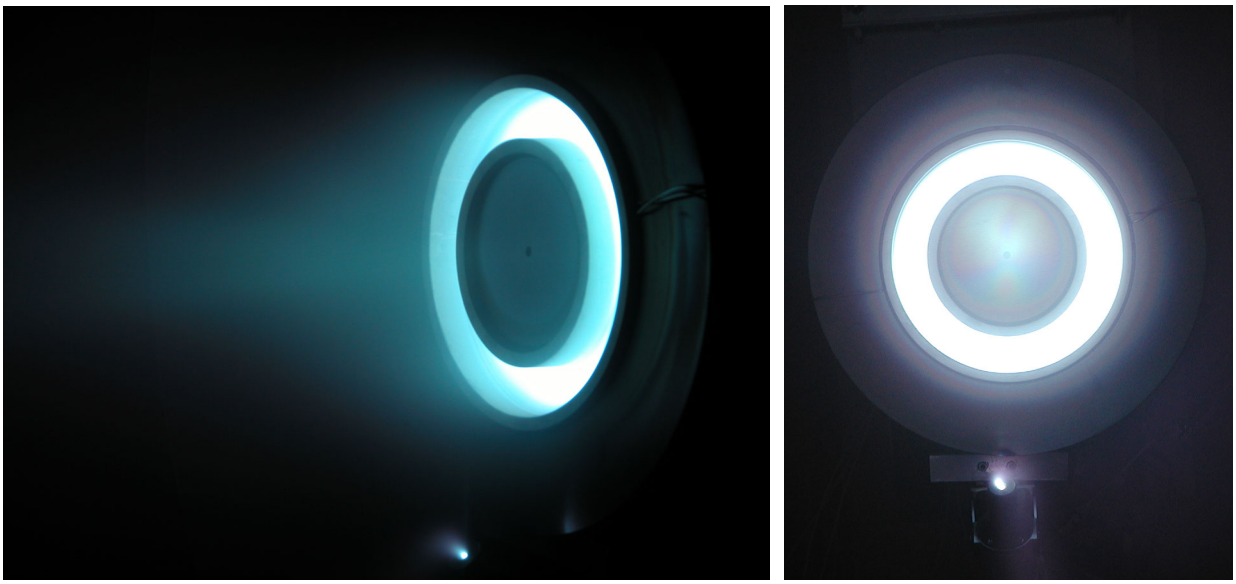

Fig. 12 Thruster firing in Alta IV-4 facility.

7. CONCLUSIONS

Although very basic and prototypical in its configuration, the designed HET proved to be a valid test bench for validating the design methods and tools developed by Alta and Centrospazio. Indeed, in spite of the mentioned issue related to propellant injection, of the design philosophy which privileged ease of manufacturing and low-cost, and of the still not optimised operating point (especially considering the three independently powered coils), the thruster demonstrated a fair overall performance with peak total efficiency of 0.49 at 3.6 kW (thrust 204 mN thrust, and specific impulse 2000 s). As of January 2003, the total cumulative firing time achieved on the thruster was about 20 hours.

A first step in the performance improvement is now being pursued, with a new anode being manufactured and a series of optimisation runs on the magnetic coils. Also, exploration of thruster operation at higher discharge voltage will be performed, and plume ion current distribution will be mapped, in order to provide a better understanding of the thruster behaviour.

8. ACKNOWLEDGEMENT

The authors wish to acknowledge the support of the Qinetiq's Space Department for kindly making available a cathode/neutralizer unit for the purpose of these tests. The help of A. Passaro (Centrospazio-CPR) was also essential for DSMC simulation of neutral injection conditions.

The activities herein presented were partially funded by Agenzia Spaziale Italiana (ASI) under contract ARS-CI-98-10, and by European Space Agency (ESA) under contract 16223/02/NL/PA (officer J. Gonzalez del Amo).

9. REFERENCES

1. J.M. Haas, *et al*., "Performance Characteristics of a 5kW Laboratory Hall Thruster", AIAA 98-3503, *34th Joint Propulsion Conference*, July 1998.

2. F.S. Gulczinski III, "Examination of the Structure and Evolution of Ion Energy Properties of a 5 kW Class Laboratory Hall Effect Thruster at Various Operational Conditions", Ph.D. Dissertation, University of Michigan, 1999.

3. B.A.Archipov, *et al*., "Thermal Design of the Electric Propulsion System Components: Numerical Analysis and Testing at Fakel", AIAA 98-3489, *34th Joint Propulsion Conference*, July 1998.

4. S. Roche, et al., "Thermal Analysis of a Stationary Plasma Thruster", AIAA 99-2296, 35th Joint Propulsion Conference, July 1999.

5. C.A. Lentz, and M. Martinez-Sanchez, "Transient One Dimensional Numerical Simulation of Hall Thrusters", AIAA 93-2491, *29th Joint Propulsion Conference*, July 1993.

6. D.H. Manzella, *et al*.,"Performance Evaluation of the SPT-140", IEPC-97-059, *25th International Electric Propulsion Conference*, August 1997.
7. S. Roy, and B. Pandey, "Development of a Finite Element Based Hall Thruster Model for Sputter Yield Prediction", IEPC-01-049, *27th International Electric Propulsion Conference*, October 2001.
8. R.A. Martinez, *et al*., "Experimental Investigation of Hall Thruster Magnetic Field Topography", *27th IEEE International Conference on Plasma Science*, June 2000.
9. R.R. Hofer, *et al*., "Optimization of Hall Thruster Magnetic Field Topography", *27th IEEE International Conference on Plasma Science*, June 2000.

APPENDIX

Table A-1 – Performance data (*anode efficiency* is computed considering the discharge power and the anode mass flow rate only, *discharge efficiency* considering both the anode and cathode mass flow rate, *overall efficiency* considering also the magnets power of 450 W).

AMFR [mg/s Xe]	CMFR [mg/s Xe]	Discharge Voltage [V]	Discharge Current [A]	Discharge Power [W]	Thrust [mN]	Specific Impulse [s]	Anode Efficiency	Discharge Efficiency	Overall Efficiency
6,00	0,40	350	6,85	2398	119	1895	0,492	0,461	0,389
6,00	0,40	375	7,20	2700	132	2102	0,538	0,504	0,432
6,00	0,40	250	6,60	1650	88	1402	0,391	0,367	0,288
6,00	0,40	350	6,66	2331	116	1848	0,481	0,451	0,378
6,00	0,40	350	6,56	2296	114	1816	0,472	0,442	0,370
6,00	0,40	350	6,49	2272	119	1895	0,520	0,487	0,407
6,00	0,40	375	6,35	2381	118	1879	0,487	0,457	0,384
6,00	0,40	325	6,55	2129	110	1752	0,474	0,444	0,367
6,00	0,40	300	6,36	1908	107	1704	0,500	0,469	0,379
6,00	0,40	275	6,19	1702	98	1561	0,470	0,441	0,349
6,00	0,40	250	6,44	1610	92	1465	0,438	0,411	0,321
6,00	0,40	375	7,10	2663	116	1848	0,421	0,395	0,338
6,00	0,40	350	6,90	2415	115	1832	0,456	0,428	0,361
6,00	0,40	325	6,49	2109	117	1864	0,541	0,507	0,418
6,00	0,40	300	6,71	2013	107	1704	0,474	0,444	0,363
6,00	0,40	275	6,32	1738	100	1593	0,479	0,450	0,357
6,00	0,40	350	6,50	2275	118	1879	0,510	0,478	0,399
8,00	0,40	250	9,30	2325	120	1456	0,387	0,369	0,309
8,00	0,40	275	9,60	2640	145	1760	0,498	0,474	0,405
8,00	0,40	300	9,60	2880	157	1905	0,535	0,509	0,441
8,00	0,40	325	9,66	3140	168	2039	0,562	0,535	0,468
8,00	0,40	350	9,72	3402	174	2112	0,556	0,530	0,468
10,00	0,40	375	12,20	4575	216	2117	0,510	0,490	0,446
10,00	0,40	350	11,40	3990	210	2058	0,553	0,531	0,478
10,00	0,40	325	12,50	4063	207	2029	0,527	0,507	0,457
10,00	0,40	300	12,20	3660	204	2000	0,569	0,547	0,487
10,00	0,40	275	12,20	3355	194	1902	0,561	0,539	0,476
10,00	0,40	250	11,85	2963	175	1715	0,517	0,497	0,431
10,00	0,40	350	12,10	4235	212	2078	0,531	0,510	0,461